PHYSICS

Unraveling the physiochemical nature of colloidal motion waves among silver colloids

Xi Chen[1]†, Yankai Xu[2]†, Chao Zhou[1], Kai Lou[3], Yixin Peng[1], H. P. Zhang[2]*, Wei Wang[1]*

Traveling waves are common in biological and synthetic systems, including the recent discovery that silver (Ag) colloids form traveling motion waves in H_2O_2 and under light. Here, we show that this colloidal motion wave is a heterogeneous excitable system. The Ag colloids generate traveling chemical waves via reaction-diffusion, and either self-propel through self-diffusiophoresis ("ballistic waves") or are advected by diffusio-osmotic flows from gradients of neutral molecules ("swarming waves"). Key results include the experimental observation of traveling waves of OH^- with pH-sensitive fluorescent dyes and a Rogers-McCulloch model that qualitatively and quantitatively reproduces the key features of colloidal waves. These results are a step forward in elucidating the Ag-H_2O_2-light oscillatory system at individual and collective levels. In addition, they pave the way for using colloidal waves either as a platform for studying nonlinear phenomena, or as a tool for colloidal transport and for information transmission in microrobot ensembles.

INTRODUCTION

Oscillatory processes are ubiquitous in living systems (*1*–*5*), such as the circadian rhythm (*6*), beating cardiac pacemaker cells (*7*), glycolytic oscillation of yeast cells (*8*), and cytosolic oscillation in Min proteins (*9*), to name a few. The coupling between oscillatory units often leads to synchronization (*10*–*14*), and a synchronized population with phase lags then gives rise to traveling waves, such as calcium waves spreading across a fertilized egg (*10*), action potentials propagating among beating heart cells (*11*), mitotic states spreading across *Xenopus* cytoplasm (*12*), and waves of self-organizing amoeba *Dictyostelium discoideum* (*13*). Similar waves are also plentiful in synthetic systems such as Belousov-Zhabotinsky (BZ) reactions (*14*–*17*), catalytic reactions on the surface of platinum (*18*, *19*), and biochemical reaction networks of enzymatic and DNA hybridization reactions (*20*). Unraveling the physiochemical nature of these waves is important for both fundamental and applied reasons.

The recent discoveries of photochemically active, oscillating silver-containing colloids (*21*–*25*) have ushered in a new member to this exciting family of nonlinear processes. An inert polymer microsphere half-coated with silver (an "active colloid"; Fig. 1A), when immersed in an aqueous solution of H_2O_2 and KCl and exposed to light sources with wavelengths shorter than green, alternates between a fast motion away from its Ag cap and a slow resting stage (*21*, *22*). Figure 1B and movie S1 display typical examples of such "pulses." Earlier studies from the Sen lab (*21*), and later from us (*22*), have hypothesized that the photodecomposition of AgCl and the oxidation of Ag back to AgCl oscillate on the particle surface via

$$2AgCl + H_2O \xrightarrow{\text{UV light}} 2Ag + 1/2\,O_2 + 2H^+ + 2Cl^- \quad (1)$$

$$2Ag + H_2O_2 + 2Cl^- \rightarrow 2AgCl + 2OH^- \quad (2)$$

To understand why this pair of reactions oscillates, we and the Sen lab proposed that the Ag nanoparticles produced in Eq. 1 serve as catalytic hotspots that further decomposes AgCl, making Eq. 1 autocatalytic (*22*). The negative feedback comes from the finite supply of AgCl on the particle surface. However, as we shall see below, new evidence suggests that OH^- renders Eq. 2 autocatalytic, instead of Eq. 1. Regardless of the chemical detail, the diffusion of chemicals from Eqs. 1 and 2 propels the Janus particles via self-diffusiophoresis (*26*). Because reactions are oscillatory, so are the colloidal motion.

More pertinent to the current discussion, however, these chemicals serve as messengers that synchronize a colloidal population (*23*). Such a synchronized population with phase lags then produces periodic motion waves that propagate across the entire population (Fig. 2A) (*21*). This is manifested in sequential bands of colloids that either self-propel ballistically in all directions ("ballistic waves;" Fig. 2B) (*27*) or move back and forth in a coordinated fashion ("swarming waves"; Fig. 2C). One captivating feature of such colloidal motion waves is the rapid information transmission that does not decay or be distorted over distance or time and without external intervention, which is helpful in the spatiotemporal control of microscopic swarms (*28*–*34*). Despite recent efforts in elucidating the

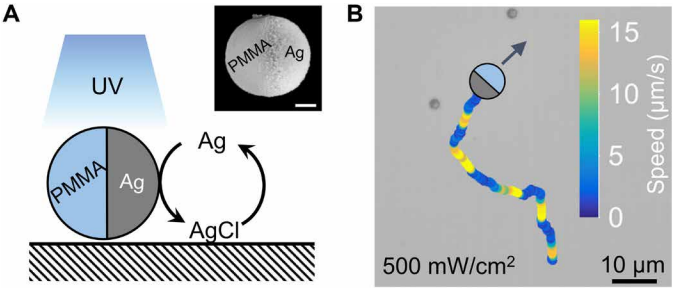

Fig. 1. Oscillating colloids. (**A**) A polymethylmethacrylate (PMMA) microsphere half-coated with silver (Ag) undergoes an oscillatory chemical reaction between Ag and AgCl in the presence of UV light, H_2O_2, and KCl (not shown). Inset: scanning electron micrograph of the PMMA-Ag Janus sphere; scale bar, 0.5 μm. (**B**) A representative trajectory of a PMMA-Ag Janus colloid that oscillates between episodes of fast and slow motion. Its instantaneous speeds are color-coded.

[1]Sauvage Laboratory for Smart Materials, School of Materials Science and Engineering, Harbin Institute of Technology (Shenzhen), Shenzhen 518055, China. [2]School of Physics and Astronomy and Institute of Natural Sciences, Shanghai Jiao Tong University, Shanghai 200240, China. [3]Guangzhou Kayja-Optics Technology Co. Ltd., Guangzhou 511458, China.
*Corresponding author. Email: weiwangsz@hit.edu.cn (W.W.); hepeng_zhang@sjtu.edu.cn (H.P.Z.)†These authors contributed equally to this work.

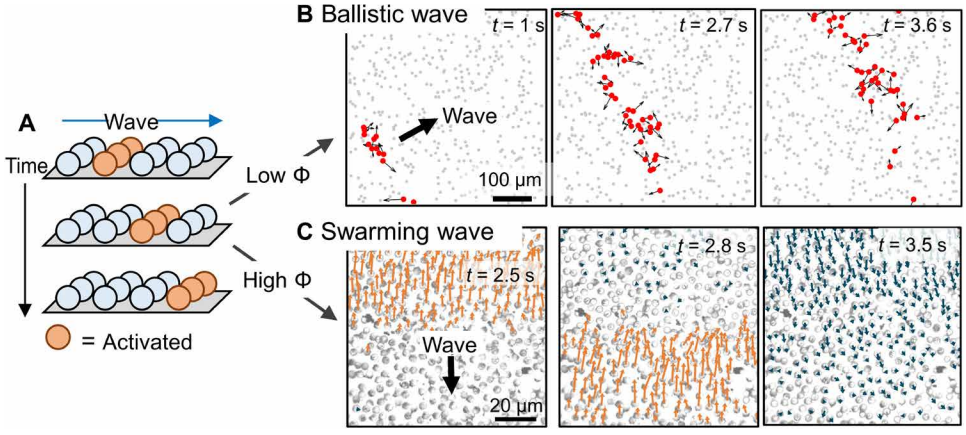

Fig. 2. Ballistic and swarming colloidal waves. (**A**) Schematic diagram of a colloidal motion wave propagating to the right. Each sphere is half-coated with Ag that is not drawn. (**B**) Ballistic wave propagating across a population of PMMA-Ag colloids. Activated colloids are marked with red dots and their velocities are labeled with arrows. ϕ = 1.3%. This figure came from figure 1D in (*27*). Copyright 2021, Royal Society of Chemistry. (**C**) Swarming wave propagating downward. Particle velocities are labeled with arrows, so that those moving toward an incoming wave are in orange and those trailing a wave are in dark blue. ϕ = 29%.

chemical pathways underpinning the intriguing oscillation (*22*) and the synchronization process (*23*) of this Ag-H_2O_2-light oscillatory system, the physiochemical nature of colloidal waves remains poorly understood.

This article tackles this fundamental question. We begin with qualitative (Fig. 2) and quantitative (Fig. 3) descriptions of the main features of a colloidal wave, with an emphasis on swarming waves. Fluorescence imaging reveals the presence of a traveling OH^- gradient (Fig. 4), suggesting the propagation of chemical waves that activate a colloidal population. An activated colloid at a wavefront either self-propels at low population densities or traces neutral diffusio-osmosis at high population densities, giving rise to ballistic and swarming waves, respectively (Fig. 5). The transition is believed to be due to rising ionic strength in a crowded population undergoing continued reactions. A reaction-diffusion model with an interplay between an activator and an inhibitor species (Fig. 6) agrees with experimental results both qualitatively (Fig. 7) and quantitatively (Fig. 8). The physiochemical nature of colloidal waves is summarized in Discussion, along with discussions on the limitations of our models, necessary ingredients of colloidal waves, how our observations compare to existing reports of chemical and colloidal waves, and their potential applications.

Overall, this article presents a first peek into how chemically active colloids generate and respond to chemical waves, in ways beyond classic reaction-diffusion systems such as BZ reactions. Our findings show the rich possibilities of connecting active matter to nonlinear sciences and inspire biomimetic strategies for the swarm control of microscopic machines.

RESULTS

Characterizing colloidal waves

A synchronized population of oscillating, Ag-containing colloids generate periodic colloidal motion waves (Fig. 2). Previously (*27*), we have reported ballistic waves at an intermediate population density [e.g., two-dimensional (2D) packing fraction ϕ ~ 1.3%], where activated colloids at a wavefront move ballistically in all directions as a result of their phoretic self-propulsion (Fig. 2B and movie S2). The speeds of such a wave scale inversely with the medium viscosity [figure 4B in (*27*)], suggesting that these are triggered rather than phase waves.

A qualitatively different type of wave, termed swarming wave, emerges at even higher population densities, and a typical example is given in Fig. 2C (movie S3). In this example, polymethylmethacrylate (PMMA) microspheres half-coated with silver ("PMMA-Ag") at a ϕ of ~29% were suspended in 0.5 weight % (wt %) H_2O_2, 200 μM KCl and illuminated with 365-nm light of 43 mW/cm^2. Note that any colloidal particle containing Ag would, in principle, generate swarming waves, even if not Janus (see Discussion for details). Figure 2C shows a motion wave propagating from the top of the field of view to the bottom, taking the form that a narrow band of PMMA-Ag spheres moved all at once toward the incoming wave, then gradually slowed down and moved backward, followed by the particles next in line along the wave direction. This is similar to the so-called "Mexican wave" found in a football stadium (*35*), where spectators move in sequence and produce wave-like motion circulating the whole stadium.

This swarming wave is further quantified in Fig. 3 by single-particle tracking and micro–particle image velocimetry (micro-PIV), which considers colloidal particles as flow tracers (this turns out to be an accurate description as we elaborate below). Results in Fig. 3 (A to C) reveal that, in this particular case, waves travel at a speed of ~160 μm/s and at a period of ~5 s. These parameters are tunable. For example, a change in light intensity only mildly changes the period and speeds of a swarming wave (Fig. 3D), yet it substantially alters the ensemble dynamics of waves (fig. S1 and movie S5). Moreover, a wave travels faster at higher population densities (Fig. 3E), possibly because of the now shorter distance for the chemical message to diffuse before reaching the next particle.

Swarming waves are distinct from ballistic waves in two ways. First, Janus colloids in a swarming wave diffused in random directions in the absence of a wave but moved in the same direction as a wave passes regardless of their individual Janus orientations (see fig. S2, C and D, for details). Activated colloids in a ballistic wavefront, on the other hand, move to directions prescribed by their Janus orientations. Second, Fig. 3F shows that colloidal particles swarm faster in a more crowded population, whereas ballistic waves show the

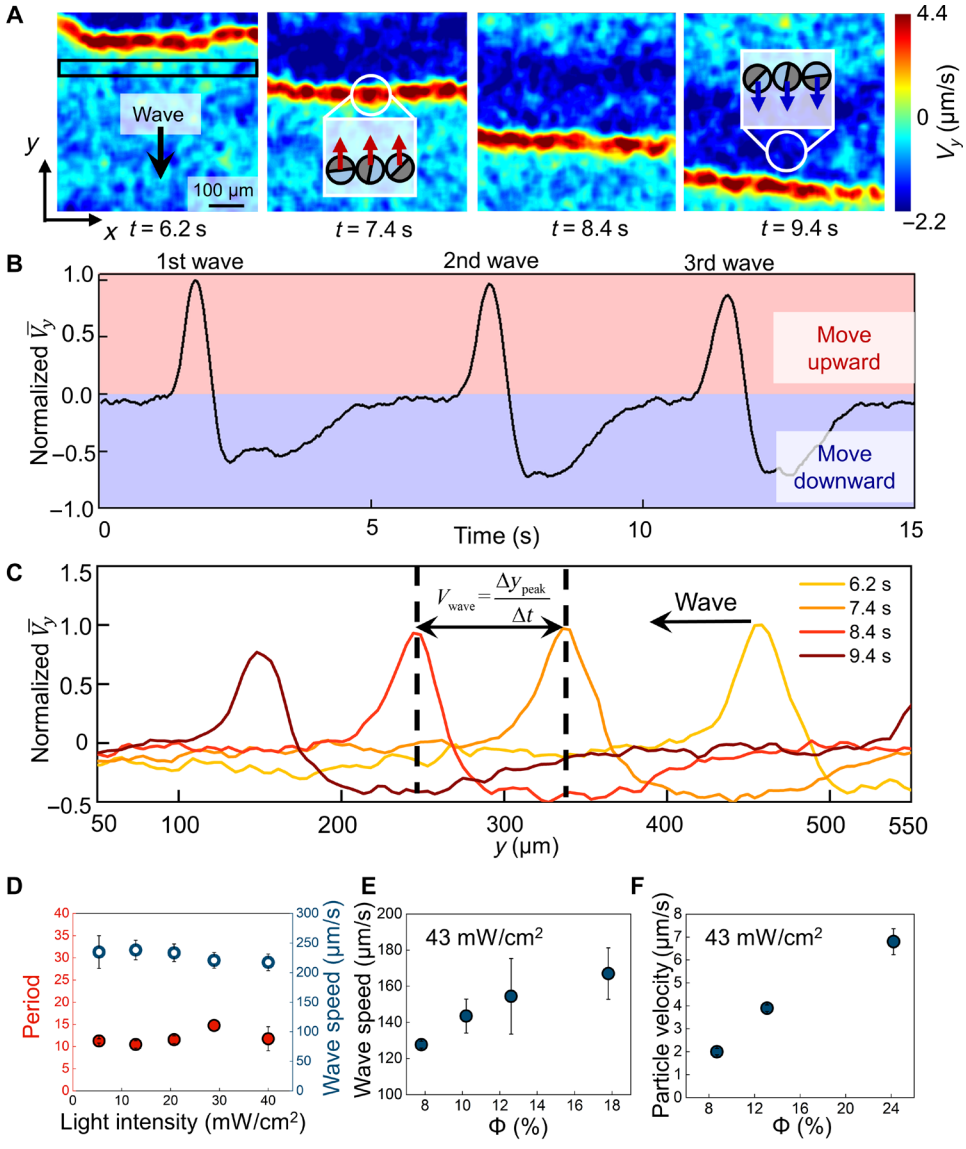

Fig. 3. Quantitative characterization of a swarming wave. (**A**) Micro-PIV–generated flow velocities along the *y* direction (V_y) of a population of PMMA-Ag particles during the downward propagation of a wave. Positive (upward) velocities are colored red and negative velocities are colored blue. Cartoons in the insets represent how colloids move at or after a wavefront. (**B**) Normalized V_y averaged across the rectangular box labeled in (A) during the downward propagation of three consecutive waves. Wave periods are calculated by finding the time differences between the peaks. (**C**) Normalized flow velocities averaged over *x* at four different time instances labeled in (A) as one wave propagates along *y*. Wave speed, V_{wave}, is calculated by dividing the distance the wavefront travels along *y* (Δy_{peak}) by the time interval Δt. (**D**) Wave periods and speeds under different light intensities. (**E**) Wave speeds at different population densities ϕ. (**F**) Particle speeds at different population densities. Error bars represent SDs from three measurements; 0.5 wt % H_2O_2 and 200 μM KCl were used in all experiments in this figure.

opposite trend [see figure 3C in (*27*)]. Both observations suggest that colloids are collectively swept in a swarming wave but self-propelling in a ballistic wave. The physiochemical reasons for these differences are given below.

What governs the origin and directionality of a colloidal wave? Our preliminary results from both experiments and simulations suggest that waves tend to originate from denser patches of particles (results not shown), possibly arising from the inevitable nonuniformity and/or thermal fluctuation. Once generated, a wavefront always propagates outward, either in concentric circles or in spirals (see Fig. 7, A and C). Waves are unidirectional because once an Ag particle becomes activated (excited), it needs a certain time to recover before it can be activated again (i.e., a refractory period). For the same reason, two colloidal waves annihilate and disappear (Fig. 7E). The physiochemical nature of such "activation" and "recovery" is proposed below.

Physiochemical nature of a colloidal wave: Chemical waves

Inspired by traveling waves commonly found in reaction-diffusion systems, we hypothesize that the above colloidal waves are underpinned by a traveling chemical wave out of a reaction-diffusion process. More specifically, we suspect that a rise of local OH^- concentrations

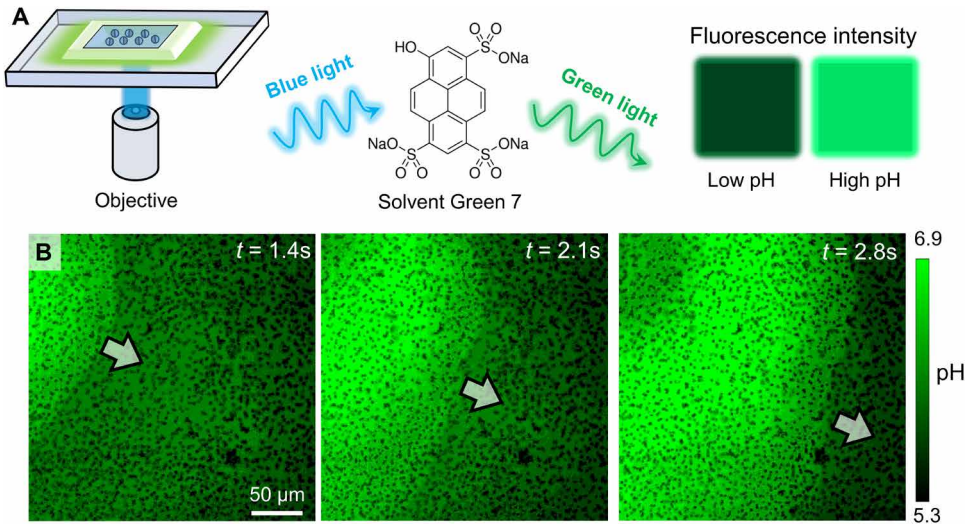

Fig. 4. Experimental confirmation of an OH^- wave. (**A**) Schematic diagram of the experimental setup for relating the fluorescence emission of Solvent Green 7 with local pH. (**B**) Optical micrographs of the pH profile during the propagation of a colloidal wave. PMMA-Ag particles of a population density ϕ of 25% were suspended in an aqueous solution containing 0.5 wt % H_2O_2, 200 μM KCl, and 100 μM Solvent Green 7. A blue light source (475 nm, 75 mW/cm^2) served both to activate the oscillatory reaction and to excite the dye molecules.

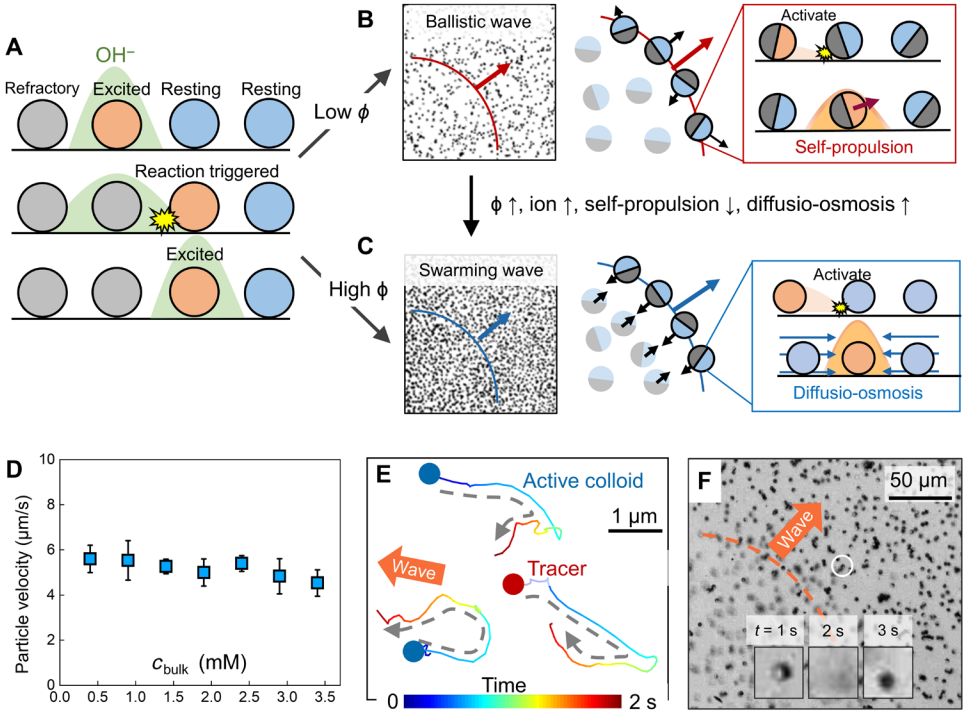

Fig. 5. Physiochemical nature of colloidal waves. (**A**) A traveling OH^- field triggers the autocatalytic oxidation of Ag on the particle surface and keeps the chemical wave propagating. (**B**) Particles activated by a chemical wave in a less crowded population self-propel away from their Ag cap, forming a ballistic wave. (**C**) Colloidal waves shift from being ballistic to being swarming as population densities increase, because self-propulsion is reduced by an increase in ionic strength, while diffusio-osmosis intensifies with an increase in the gradient of neutral molecules at high population densities. (**D**) Particle velocities at a wavefront decrease slightly upon increasing the salt (KNO_3) concentration in the bulk solution. Error bars represent SDs from three measurements. (**E**) Actual trajectories (color-coded in time) of one polystyrene tracer and two Janus colloids during the passage of one colloidal wave. (**F**) Particles move upward and out of focus as a wave sweeps across them. Inset: zoomed-in views of one particle circled in white over time. In all experiments, PMMA-Ag particles [population density ϕ of 21% for (E) and 14% for (F)] were suspended in an aqueous solution containing 0.5 wt % H_2O_2 and 200 μM KCl under a UV illumination of 43 mW/cm^2.

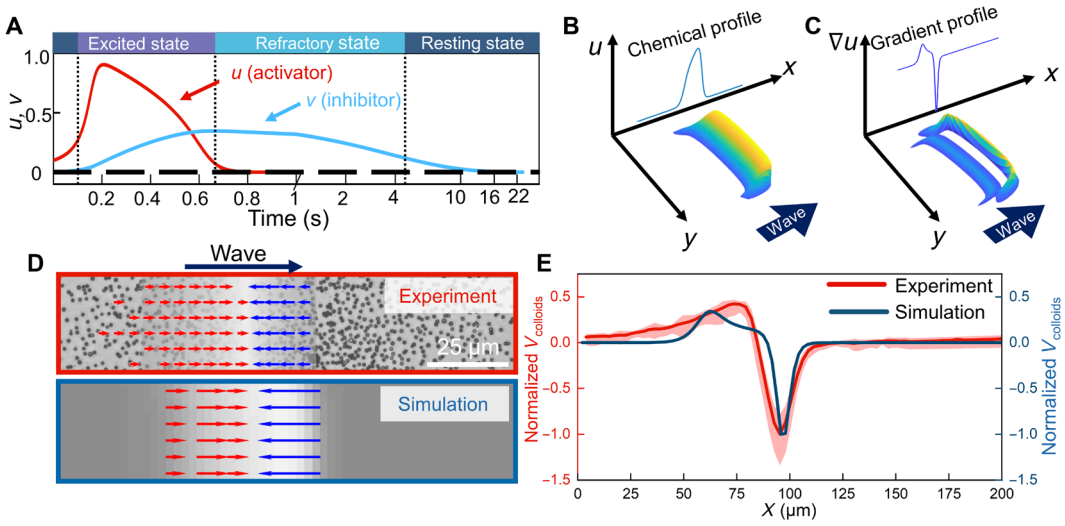

Fig. 6. Simulating colloidal waves as a reaction-diffusion process. (**A**) The temporal variation of the concentrations of the activator (*u*) and the inhibitor (*v*) shows three states. The concentration of the activator *u* and its gradient ∇u propagating forward in the *x*-*y* plane are shown in (**B**) and (**C**), respectively. The direction (**D**) and magnitude (**E**) of the particle velocity (*V*) at a wavefront can be related between experiments and simulations via $V \propto \nabla u$. In the experiments shown in (D) and (E), PMMA-Ag particles of a population density ϕ of 19% were suspended in an aqueous solution containing 0.5 wt % H_2O_2 and 200 μM KCl under a 405-nm illumination of 1.6 W/cm^2.

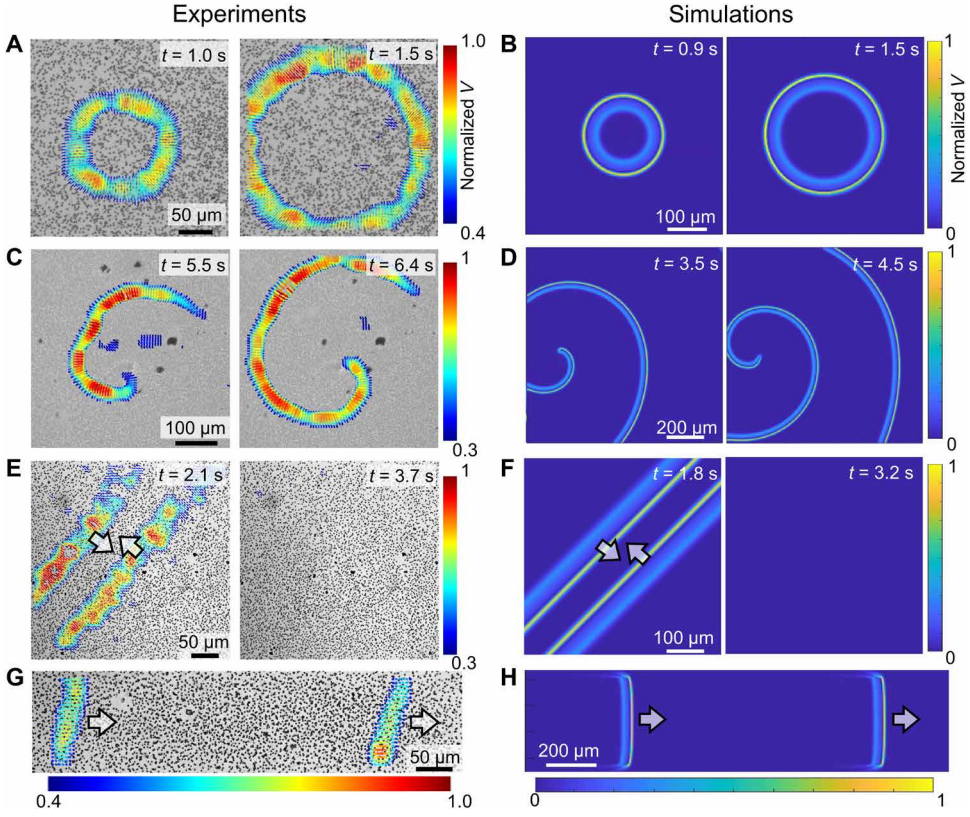

Fig. 7. Qualitative comparison of colloidal waves between experiments (left) and simulations (right). (**A** to **D**) Evolution of target waves (A and B) and spiral waves (C and D). (**E** and **F**) The annihilation of two colloidal waves traveling in opposite directions. (**G** and **H**) Two consecutive waves. In all experiments, PMMA-Ag particles [population density ϕ of 20% for (B), 15% for (D), 20% for (F), and 23% for (H)] were suspended in an aqueous solution containing 0.5 wt % H_2O_2 and 200 μM KCl under a 405-nm illumination of 1.6 W/cm^2. See the Supplementary Materials for simulation details and the choice of parameters.

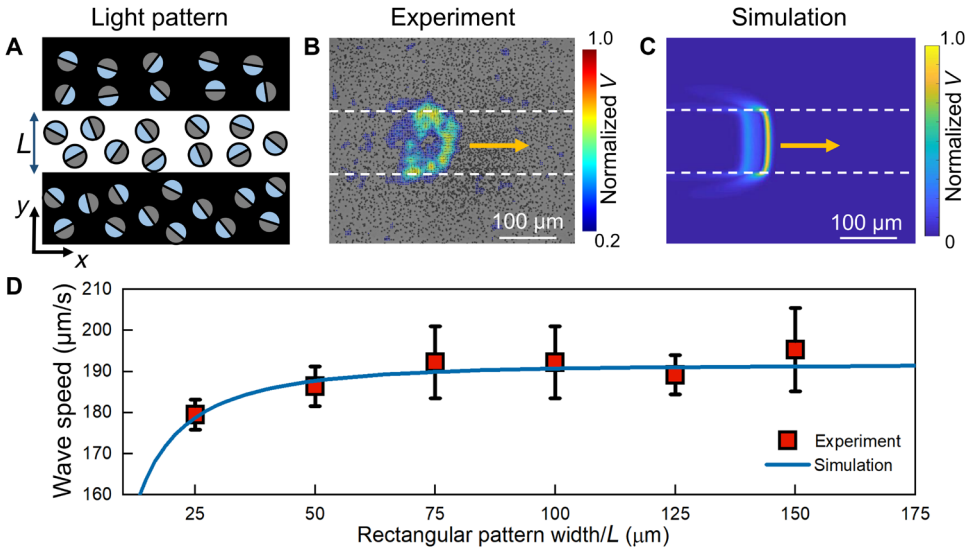

Fig. 8. Quantitative comparison between experiments and simulations for wave speeds traveling in light patterns. (**A**) Schematic of a rectangular light pattern of 490 × 100 μm projected on a population of Janus PMMA-Ag microspheres. (**B**) Micro-PIV tracking of a colloidal wave propagating along the long axis of the light pattern. The yellow arrows represent the wave direction. (**C**) A simulated wave traveling in the same light pattern as (B). See the Supplementary Materials for simulation details and the choice of parameters. (**D**) Experimental and simulated wave speeds in light patterns of different widths (*L*). Error bars represent SDs from three measurements. In all experiments, PMMA-Ag particles of a population density ϕ of 19% were suspended in an aqueous solution containing 0.5 wt % H_2O_2 and 200 μM KCl under a 405-nm illumination of 1.6 W/cm^2.

is autocatalytic. To elaborate, H_2O_2 is known to decompose faster at high pH (*36*), during which a burst of highly oxidative intermediates such as OH· or OOH·(*37*, *38*) could be generated that oxidize Ag into AgCl. More OH^- are then produced by Eq. 2, thus comprising a positive feedback loop. As a result, a rise of local pH "activates" a Ag-containing colloid (see Fig. 5A below) to release a burst of chemicals, replenishing the chemical gradient that has already decayed and keeping the chemical wave propagating. Over time, however, most Ag is converted to AgCl, which decomposes slowly under light to yield Ag and in the process lowers pH. This is the negative feedback, and a colloidal particle is covered mostly by AgCl and at a low pH is in its "refractory" state and cannot be activated.

The key evidence of this OH^--mediated mechanism is the presence of chemical waves of OH^-. To this end, we measured the spatiotemporal distribution of local pH with a pH-sensitive fluorescent dye Solvent Green 7 (Fig. 4A), the emission of which intensifies monotonically with an increase in pH (see fig. S3 for calibration). Waves of green fluorescence (Fig. 4B and movie S6) periodically propagated among Ag colloids, suggesting a traveling concentration profile of OH^- that is higher behind a wave than in front of it. Figure S4 further shows that the spatiotemporal profiles of the chemical waves match that of the concurrent colloidal waves.

The production of OH^- most likely comes from the oxidation of Ag into AgCl by H_2O_2, (Eq. 2). This was confirmed by simply mixing Ag colloids with KCl and H_2O_2 in the absence of light (i.e., only Eq. 2 but not Eq. 1). The global pH value rapidly increased from 5.9 to 9.6 in 1 min upon the addition of 0.5 wt % H_2O_2 (fig. S5A). The decrease in fluorescence intensity behind a wave, on the other hand, is likely due to the production of H^+ during the photodecomposition of AgCl into Ag (Eq. 1). This is confirmed by a rapid decrease in the solution pH in an aqueous suspension of AgCl microparticles under ultraviolet (UV) light in the absence of H_2O_2 (fig. S5B). The above fluorescence mapping and accompanying pH measurements in the bulk strongly suggest that the oxidation of Ag and the photodecomposition of AgCl occur at and behind a wavefront, respectively.

A few other pieces of experimental evidence also support our hypothesis. First, bubbles were produced as colloidal waves passed (movie S7), suggesting that H_2O_2 decomposed faster as waves sweep by, in agreement with a rise of local pH. Second, we observed a single fluorescent wave upon turning off the light (movie S8), which indicates that the fast reaction at a wavefront does not require light, consistent with Eq. 2 but not Eq. 1. Last, fig. S6 shows that the oscillation frequency of an individual Ag colloid, as well as that of a colloidal wave, increases upon increasing the bulk pH, consistent with the hypothesis that OH^- accelerates the chemical clock of colloids.

Physiochemical nature of a colloidal wave: Colloids respond to a chemical wave

The exact way a colloidal particle responds to a chemical wave dictates the type of colloidal wave. Upon being triggered by a chemical wave, and at a relatively low population density (yet still high enough to enable waves), a Ag-containing colloidal particle establishes a gradient of ions across its Janus body and undergoes ionic self-diffusiophoresis (*22*, *39*), which propels it away from its Ag cap (Fig. 5B). A band of Janus colloids then move in directions prescribed by their own Janus orientations, collectively exhibiting a ballistic wave. The electrokinetic nature of a ballistic wave is best supported by a sharp decrease of colloidal speed upon adding salt (fig. S7), a hallmark feature commonly seen in colloidal motors or pumps powered by self-electrophoresis or ionic diffusiophoresis (*39*–*42*).

At an even higher population density, however, Ag colloids produce more ions that further raise the solution ionic strength, which weakens all electrokinetic effects as stated above and reduces self-propulsion. This sharp decrease in speeds of diffusiophoretic colloidal motors at high population densities has been confirmed in our recent study (*43*). On the other hand, as H_2O_2 quickly decompose

to O_2 in a rising pH, chemical gradients of neutral molecules give rise to local osmotic flows known as neutral diffusio-osmosis (*44*), which moves colloidal particles via advection in addition to their own self-propulsion. As self-propulsion weakens and diffusio-osmosis intensifies in a crowded population with a rising ionic strength, the form of a colloidal wave switches to a swarming wave, where each colloid is chemically but not phoretically active, and traces a local osmotic flow (Fig. 5C). Note that there is unlikely a "critical population density" for such transition to occur, because we have observed colloidal waves that exhibit both features at intermediate ϕ (see fig. S2 and movie S4 for an example).

The magnitude of neutral diffusio-osmotic flow velocity V, and thus that of the advected colloids, is proportional to the local chemical gradient ∇c of neutral molecules via (*44*)

$$V = -\frac{k_B T}{\eta} K L^* \nabla c \tag{3}$$

where k_B is the Boltzmann constant, T is the temperature (in kelvin), and η is the dynamic viscosity of the medium. The parameters K and L^* together determine the direction and strength of the solute-surface interaction. Notably, Eq. 3 suggests that the magnitude of neutral diffusio-osmosis is insensitive to the ionic strength, making it the more viable way for a colloidal particle to move in high ionic strength.

Five compelling pieces of evidence support the dominance of diffusio-osmosis in a swarming wave. First, an earlier calculation has yielded a negative value for $K{\cdot}L^*$ of O_2 gradients [see appendix I in (*41*)], meaning that diffusio-osmosis moves colloids up the O_2 gradient. Similar diffusio-osmosis during the catalytic decomposition of H_2O_2 have also been reported (*45*, *46*). Since we propose that more O_2 is produced at the wavefront, Eq. 3 then predicts that diffusio-osmosis would advect colloids toward a wavefront from both sides, in agreement with our experiments (e.g., Figs. 2C and 3A). Second, Fig. 5D shows that the speeds of colloids at a wavefront are largely insensitive to increasing ionic strength, and Fig. 3F shows that they instead increase upon increasing the colloid population density. Both are consistent with neutral diffusio-osmosis (*44*), but not with electrokinetic effects such as electrophoresis or ionic diffusiophoresis that rely on electric fields (*42*, *47*). Third, fig. S2 (C and D) shows that the orientations of active colloids (i.e., which side is pointing to which direction) during a colloidal wave are not correlated to each other or the direction of the wave, even though they move collectively toward the same direction. This is consistent with advective transport via osmosis rather than self-propulsion. Fourth, Fig. 5E shows that active (PMMA-Ag colloids) and passive colloids (polystyrene tracers) move in a swarming wave in the same way, consistent with osmosis but not phoresis or self-propulsion given how different these two types particles are. Last, Fig. 5F and movie S9 show that colloids move upward and out of focus as waves sweep across them, consistent with osmotic flows that converge from both sides onto a wavefront.

Modeling a reaction-diffusion colloidal wave

Our proposed mechanism for colloidal waves can be corroborated by and reproduced with numerical simulations based on a reaction-diffusion principle. The first step is to model a chemical wave. As details of the underlying chemical dynamics are not completely understood, which prevents us from constructing a model from microscopic details, we instead used one of the simplest phenomenological models: the Rogers-McCulloch model (*48*). This model is based on the FitzHugh-Nagumo model and similar to the Boissonade–De Kepper model, which played a key role in the design of chemical oscillators (*15*). The Rogers-McCulloch model deals with the reaction-diffusion of two variables (*49*), the concentration of an activator species (termed u) that promotes the chemical reaction in the oscillating system, and that of an inhibitor (termed v) that suppresses the reaction. The kinetics of the spatiotemporal variation of u and v is given by (see below for explanations)

$$\frac{\partial u}{\partial t} = \nabla \cdot D \nabla u + c_1 u(u - u_c)(1 - u) - c_2 uv \tag{4}$$

$$\frac{\partial v}{\partial t} = \varepsilon(u - kv - b) \tag{5}$$

with a closed boundary condition (**n** being the unit vector normal to the boundary of our computational domain)

$$\frac{\partial u}{\partial \boldsymbol{n}} = 0 \tag{6}$$

The first term on the right-hand side of Eq. 4, $\nabla \cdot D \nabla u$, represents the diffusion of the activator with a diffusivity D. The second term $c_1 u(u - u_c)(1 - u)$ corresponds to the autocatalytic buildup u when it is raised beyond a threshold value u_c. The upper limit of u is set to be the unit concentration so that both u and v are nondimensionalized. The third term $-c_2 uv$ represents the decay of u because of the inhibitor. Constants c_1 and c_2 are the weight of the promoting/inhibiting effect by the activator and the inhibitor, respectively.

Equation 5 describes the temporal variation of v. The parameter ε is chosen to be small, so that v responds to chemical reactions more slowly than u, thereby allowing u to build up quickly. k and b in Eq. 5 are reaction constants. Note that the diffusion of the inhibitor is assumed to be very slow and not important to a wave, thus the lack of a diffusion term in Eq. 5. Key assumptions of this model and how it can be improved to match experiments are presented in Discussion.

By solving Eqs. 4 to 6, a chemical wave is reproduced in Fig. 6 (A to C), with the activators at the wavefront diffusing and triggering the reaction in a nearby area, generating more activators that then diffuse and activate the next area in line. Unless otherwise noted, one particular set of nondimensional parameters ($u_c = 0.0075$, $c_1 = 2.5$, $c_2 = 2.4$, $\varepsilon = 0.033$, $k = 0.25$, $b = 0$, and $D = 1.2$) is used throughout the article. These parameters were determined by comparing numerical and experimental results of waves under various conditions (see details in the Supplementary Materials) until differences are minimized.

Next, the simulated gradient profiles (e.g., Fig. 6C) were related to the actual velocity profiles of colloids within a swarming wave via Eq. 3, which states that colloids trace a neutral osmotic flow with a velocity $V(x, y, t)$ that scales linearly with $\nabla u(x, y, t)$. This correlation is first confirmed qualitatively by examining how the velocity vectors of colloids point perpendicular to a wavefront in both experiments and simulations (Fig. 6D) and then quantitatively by comparing the normalized colloidal velocity from both experiments and simulations (Fig. 6E). Building upon this correlation, a simulate chemical wave can be mapped to a colloidal wave (as shown in Figs. 7 and 8), even though colloidal motion is not explicit in our models.

Our numerical models can qualitatively reproduce key features of colloidal waves (Figs. 7 and 8 and movie S10), such as target waves

(Fig. 7, A and B), spiral waves (Fig. 7, C and D), two colliding waves (Fig. 7, E and F), two consecutive waves (Fig. 7, G and H), and the propagation of waves in light patterns (Fig. 8, A to C). More quantitatively, our simulations reproduced key parameters for waves travelling in rectangular (Fig. 8) or ring-shaped (fig. S8) light patterns, such as the maximum length of darkness that it can travel through (fig. S9), the minimum width of an illuminated strip for sustaining a wave (fig. S10), or how its speed varies with such width (Fig. 8D and fig. S8, G and H). The dynamics of colloidal waves in light patterns and its spatiotemporal control will be reported separately.

DISCUSSION

Limitations of modeling

Our current numerical model for simulating colloidal waves is limited in at least three aspects. First is the assumption that the reaction and diffusion take place in a continuum field, whereas oscillating reactions in actual experiments occur heterogeneously on the surface of solid microspheres. This difference could result in changes in the kinetics of chemical reactions. However, a modified model that confines reactions on the surface of discrete micro-objects (fig. S11) produced waves similar to the homogeneous model, suggesting that the emergence of chemical waves is a robust effect. Future efforts are under way to study how heterogeneity affects key features of waves such as their forms, shapes, and speeds.

The second limitation is the intentional lack of chemical details, including the chemical pathway responsible for oscillation, the reaction kinetics, and the identity of the activator and inhibitor and their diffusivity values. Although more experimental verification is clearly needed, we suspect that the activator is OH^- and the inhibitor is AgCl, because they qualitatively match the corresponding profiles prescribed by our model. For example, a rise in local pH accelerates the decomposition of H_2O_2 that not only produces more OH^- in the process (i.e., the production of the activator is autocatalytic) but also facilitates the oxidation of Ag into AgCl (i.e., the buildup of u increases v). On the other hand, the photodecomposition of AgCl reduces the local pH and thus decreases the amount of OH^- (i.e., v counteracts on u), and the diffusion of AgCl is negligible because it is attached to a microsphere (i.e., the inhibitor diffuses slowly).

The third limitation is in the way chemical waves move colloidal particles. Our simulations have related the velocity of colloids in a swarming wave with the concentration gradients of the activator via $V \propto \nabla u$. However, we have also proposed in Eq. 3 that it is the gradient of neutral molecules (such as O_2, with a concentration of c) that ultimately moved the colloids by diffusio-osmosis via $V \propto \nabla c$. Although ∇u and ∇c are likely different, we suspect that the concentration of OH^- and O_2 (i.e., u and c) likely rises together so that ∇u and ∇c are positively correlated, since a higher supply of OH^- accelerates the decomposition of H_2O_2. A more quantitative argument requires an accurate measurement of the local O_2 concentration in the same spirit of that performed in Fig. 4, as well as a better understanding of the reaction kinetics. These efforts are underway.

Despite the above limitations, the good agreement between simulation and experiments, with a single set of fitting parameters, lends strong support to the hypothesis that the interplay between the reaction and diffusion of an activator and inhibitor produces periodic chemical waves, and that these waves transport colloids via diffusio-osmosis. Results from the models therefore provide key information for unraveling the microscopic details of the chemical waves in our system in the future.

Necessary ingredients for colloidal waves to occur

For a ballistic wave to occur, an asymmetric particle (such as the Janus microsphere used above) is required to break symmetry for it to self-propel. However, this is not required for a swarming wave, because colloidal particles are in this case merely flow tracers. Swarming waves have been observed with pure Ag or Ag_3PO_4 microparticles and nanoparticles (*21*, *24*, *25*, *50*) (see movie S11 for a demonstration from our own laboratory). We have even seen it on glass slides coated with Ag (fig. S12 and movie S11; see the Supplementary Materials for details), possibly because of the Ag nanoparticles that come off the slide during reaction. A swarming wave, however, does require a neutral gradient to generate diffusio-osmosis, which is not required for a ballistic wave. Together, the necessary ingredients for colloidal waves are a system that (i) undergoes oscillatory chemical reactions, (ii) releases chemicals capable of exciting other colloids into oscillation, and (iii) produces either ions that cause ionic self-diffusiophoresis (thus, a ballistic wave) or neutral molecules that cause diffusio-osmosis (thus, a swarming wave). So far, Ag is the only material that meets all three, but materials beyond Ag are certainly possible and worth looking for.

Colloidal waves as a unique system of chemically coupled, moving oscillators

The colloidal waves reported here exhibit autonomous, periodic, and local flows that mesoscopically transport colloidal objects that are chemically coupled and is therefore noticeably different from other systems that may appear superficially similar. First, even though there have been reports of chemically propelled microswimmers with oscillating speeds, enabled by the periodic coalescence, growth, and release of large O_2 bubbles (*51*), by incorporating BZ reactions in droplets (*52*) or by periodic changes in the buoyancy during the decomposition of hydrogen peroxide (*53*), none generates colloidal waves likely because they lack an appropriate coupling mechanism in the population.

In addition, despite the presence of similar chemical waves among droplets undergoing BZ reactions (*54*), a colloidal wave is manifested by the sequential motion of colloids, which are both a source and an indicator of a propagating chemical message that is otherwise invisible to the eyes. In this sense, colloidal waves present a unique opportunity to visualize oscillating chemical reactions and the propagation of a chemical front, which typically requires chemicals with color changes to visualize.

Last, colloidal waves reported here are also qualitatively different from other types of "colloidal waves" that have been experimentally realized. For example, the Granick group reported polar waves in a population of metal-dielectric Janus colloids coupled by hydrodynamics and electrical dipolar interactions (*55*). The Zhang group recently reported fast solitary waves among dielectric colloids that start moving when close to other in a dc electric field (*56*). In both cases, singular (rather than periodic) colloidal waves are generated out of hydrodynamics and/or electromagnetic coupling, whereas periodic waves among chemically coupled colloids are found in our experiments.

Practical usefulness of colloidal waves

Although it has been demonstrated that oscillating Ag colloids can anneal colloidal crystals of inert tracers (*57*), a colloidal wave could

potentially be integrated with existing technologies, such as optical tweezers (*58*), acoustofluidics (*59*), or microfluidics (*60*), to enable even more complex manipulation of micro- and nanoscopic objects in space and time. One ongoing effort is to make such colloidal transport via motion waves more directional and controllable, inspired by recent demonstrations of other wave-mediated colloidal transport (*61*–*63*). We have, however, yet to achieve large-scale, directional colloidal transport by swarming waves, because the net displacement of a colloidal particle during one wave is exceedingly small and easily overshadowed by thermal fluctuations. This could be due to the fact that the slopes on both sides of a chemical wave are similar (e.g., Fig. 6B), which can, in principle, be tuned by engineering the chemical dynamics.

Colloidal waves could also be used in the swarm control of microrobots (*28*–*34*). Here, autonomous, periodic waves sweep across an entire microrobot population, so that they are synchronized in a way mimicking how social amoeba excrete traveling waves of chemical signals that organize them in harsh times (*13*). This very crude, yet effective, information relay system consists of a message (a chemical gradient), a transceiver (oscillating colloids), and a transmission medium/pathway (chemical diffusion). As a result, waves propagate at hundreds of micrometers per second, much faster than simple diffusion, thanks to the presence of information transmitters that continuously refresh the message. It also ensures that a clear, undistorted message reaches the far side of the group. These messages carrying information on functionalities, activities, or even shapes and forms can propagate across a microbot swarm so their operations can be modulated on the fly in a torturous environment such as human bodies.

To summarize, we have proposed the following mechanism for colloidal waves: The spontaneous oxidation of Ag into AgCl by H_2O_2 and KCl produces OH^-, which diffuses and triggers an autocatalytic burst of OH^- on nearby Ag colloids that drive them into an excited state. Soon, an already excited colloid that by now contains mostly AgCl falls into a refractory state, during which AgCl slowly decomposes under light to convert back into Ag for the next activation. The reaction and diffusion of key species such as Ag, OH^-, and AgCl out of Ag-containing colloids produce periodic, traveling chemical wave that propagates and activates more colloids. Upon activation, a Janus colloid at low population densities self-propels via ionic self-diffusiophoresis, giving rise to a ballistic wave. At higher population densities, however, ionic self-diffusiophoresis is weakened by rising ionic strength, while diffusio-osmosis from neutral gradients dominates, advecting colloids into a swarming wave. A reaction-diffusion model quantitatively agrees with the key experimental parameters of colloidal waves, such as their shapes, speeds, and dynamics in confined spaces. Traveling OH^- waves are also experimentally verified with fluorescent dyes.

Looking forward, our understanding of the physiochemical nature of a colloidal wave could lead to the development of a wave-mediated information transmission system for autonomous microrobots. Waves can also be used in conjunction with other existing techniques to transport colloids in an autonomous and programmable fashion. On a fundamental level, colloidal waves present a unique way to visualize oscillating chemical reactions and the propagation of a traveling chemical wave, and is thus a good model system of reaction-diffusion processes at mesoscopic and microscopic scales.

MATERIALS AND METHODS

Sample

PMMA microspheres (2.5 μm in diameter) were purchased from Bangs Laboratories. They were self-assembled into a monolayer following protocols in (*64*). Janus PMMA-Ag particles were prepared by evaporating 50 nm of Ag layer onto the microsphere monolayer using an E-beam evaporator (HHV TF500). These Janus particles were released by sonication and dispersed in deionized water. The preparation of pure Ag colloidal particles used for fig. S12A and movie S11 was based on the literature (*65*) by mixing silver nitrate solution (0.15 M) and ascorbic acid solution (0.09 M) with 0.5 wt % polyvinyl pyrrolidone to react at room temperatures under continuous stirring. The Ag-coated substrate for fig. S12B and movie S11 was prepared by sputtering 20-nm Ag on the glass slide.

Experimental setups and colloidal wave experiment

An inverted optical microscope (Olympus IX71) was used to observe the motion of colloidal particles. A light-emitting diode (LED) UV lamp with a central wavelength at 365 nm (Thorlabs, M365LP1-C1) was used to excite colloids from above. A ring-shaped lamp of white LED was placed around the UV lamp to provide background lighting for imaging, and we confirm that this white LED light is incapable of exciting colloids into oscillation. Light intensities were measured with power meters (Thorlabs PM 100A and S175C).

In a typical colloidal wave experiment, a suspension of PMMA-Ag colloids with certain concentrations of H_2O_2 and KCl was pipetted into a homemade chamber, which was then covered with a coverslip. After a few minutes, the majority of PMMA-Ag colloids settled down on the glass substrate. When UV light was applied, colloidal waves typically emerged after a few minutes of incubation. Particle population density was measured by calculating their packing fraction on a 2D plane using imageJ.

In the fluorescence wave experiment (Fig. 4), 100 μM pH-sensitive fluorescence dye trisodium 8-hydroxypyrene-1,3,6-trisulfonate (Solvent Green 7) was used with the oscillating colloids. The mixed suspension was irradiated with blue light (475-nm central wavelength, 75 mW/cm^2) that was produced by filtering a halogen lamp via a fluorescent cube (model FITC, excitation wavelength, 455 to 495 nm; emission wavelength, 505 to 555 nm; Optolong Optics). The blue light served both to activate the oscillating colloids and to excite the dye molecules.

In the experiments with tracer particles (e.g., Fig. 5E), we mixed fluorescent polystyrene tracers of 1 μm in diameter with the oscillating colloids. Green light (530 to 550 nm) was produced by filtering a halogen lamp via a fluorescent cube (model U-FGW, Olympus) to excite fluorescent tracers. UV light was applied to activate oscillating colloids. By carefully tuning the brightness of the background light, darker oscillating colloids and brighter tracers can be both recognized in a video.

In the colloidal wave experiments with light patterns (Fig. 8), we applied structured light to study the dynamics of the colloidal wave. The structured light has already been reported to control and manipulate microparticles (*66*, *67*), soft micro-robotics (*68*), and bacteria (*69*). Inspired by these works, we built a structured light device with a specialized projector (SICUBE, SM7-405) equipped with a 405-nm light source that can activate oscillating colloids. In addition, a 660-nm light incapable of activating oscillating colloids was also applied by an LED lamp (Thorlabs M660L4) to provide background lighting for imaging.

Particle tracking and wave visualization

The motion of Janus PMMA-Ag particles was recorded by a complementary metal-oxide semiconductor camera (GS3-U3-51S5C-C, FLIR) typically at 15 fps. These recorded videos were then analyzed by homemade MATLAB codes. The coordinates of each particle were extracted and were used to obtain trajectories and instantaneous speeds of particles. To visualize colloidal wave with micro-PIV, a video of colloidal waves was decomposed into image sequences by MATLAB and imported into Fluere, and velocity data at each node point (65×65 in a 2048 pixel $\times$ 2048 pixel image) were extracted as arrows (its color indicating the magnitude of the velocity) overlapping on the original video (Fig. 7). Alternatively, new videos can be generated without the original micrograph (Fig. 3).

SUPPLEMENTARY MATERIALS

Supplementary material for this article is available at https://science.org/doi/10.1126/sciadv.abn9130

REFERENCES AND NOTES

1. S. Kinoshita, *Pattern Formations and Oscillatory Phenomena* (Newnes, 2013).
2. M. Maroto, N. Monk, *Cellular Oscillatory Mechanisms* (Springer Science & Business Media, 2008), vol. 641.
3. M. Loose, K. Kruse, P. Schwille, Protein self-organization: Lessons from the min system. *Annu. Rev. Biophys.* **40**, 315–336 (2011).
4. C. Beta, K. Kruse, Intracellular oscillations and waves. *Annu. Rev. Condens. Matter Phys.* **8**, 239–264 (2017).
5. C. S. Colwell, Linking neural activity and molecular oscillations in the SCN. *Nat. Rev. Neurosci.* **12**, 553–569 (2011).
6. C. Dibner, U. Schibler, U. Albrecht, The mammalian circadian timing system: Organization and coordination of central and peripheral clocks. *Annu. Rev. Physiol.* **72**, 517–549 (2010).
7. I. Nitsan, S. Drori, Y. E. Lewis, S. Cohen, S. Tzlil, Mechanical communication in cardiac cell synchronized beating. *Nature Phys.* **12**, 472–477 (2016).
8. S. Kar, D. S. Ray, Collapse and revival of glycolytic oscillation. *Phys. Rev. Lett.* **90**, 238102 (2003).
9. J. Halatek, E. Frey, Highly canalized MinD transfer and MinE sequestration explain the origin of robust MinCDE-protein dynamics. *Cell Rep.* **1**, 741–752 (2012).
10. J. E. Speksnijder, C. Sardet, L. F. Jaffe, Periodic calcium waves cross ascidian eggs after fertilization. *Dev. Biol.* **142**, 246–249 (1990).
11. L. Barr, M. M. Dewey, W. Berger, Propagation of action potentials and the structure of the nexus in cardiac muscle. *J. Gen. Physiol.* **48**, 797–823 (1965).
12. J. B. Chang, J. E. Ferrell Jr., Mitotic trigger waves and the spatial coordination of the Xenopus cell cycle. *Nature* **500**, 603–607 (2013).
13. E. Pálsson, E. C. Cox, Origin and evolution of circular waves and spirals in *Dictyostelium discoideum* territories. *Proc. Natl. Acad. Sci.* **93**, 1151–1155 (1996).
14. I. R. Epstein, B. Xu, Reaction–diffusion processes at the nano- and microscales. *Nature. Nanotech.* **11**, 312–319 (2016).
15. I. R. Epstein, J. A. Pojman, *An Introduction to Nonlinear Chemical Dynamics: Oscillations, Waves, Patterns, and Chaos* (Oxford Univ. Press, 1998).
16. R. Kapral, K. Showalter, *Chemical Waves and Patterns* (Springer Science & Business Media, 2012), vol. 10.
17. K. Showalter, I. R. Epstein, From chemical systems to systems chemistry: Patterns in space and time. *Chaos* **25**, 097613 (2015).
18. H. H. Rotermund, W. Engel, M. Kordesch, G. Ertl, Imaging of spatio-temporal pattern evolution during carbon monoxide oxidation on platinum. *Nature* **343**, 355–357 (1990).
19. C. Barroo, Z.-J. Wang, R. Schlögl, M.-G. Willinger, Imaging the dynamics of catalysed surface reactions by in situ scanning electron microscopy. *Nat. Catal.* **3**, 30–39 (2020).
20. A. Padirac, T. Fujii, A. Estévez-Torres, Y. Rondelez, Spatial waves in synthetic biochemical networks. *J. Am. Chem. Soc.* **135**, 14586–14592 (2013).
21. M. E. Ibele, P. E. Lammert, V. H. Crespi, A. Sen, Emergent, collective oscillations of self-mobile particles and patterned surfaces under redox conditions. *ACS Nano* **4**, 4845–4851 (2010).
22. C. Zhou, X. Chen, Z. Han, W. Wang, Photochemically excited, pulsating janus colloidal motors of tunable dynamics. *ACS Nano* **13**, 4064–4072 (2019).
23. C. Zhou, N. J. Suematsu, Y. Peng, Q. Wang, X. Chen, Y. Gao, W. Wang, Coordinating an ensemble of chemical micromotors via spontaneous synchronization. *ACS Nano* **14**, 5360–5370 (2020).
24. A. Altemose, M. A. Sánchez-Farrán, W. Duan, S. Schulz, A. Borhan, V. H. Crespi, A. Sen, Chemically controlled spatiotemporal oscillations of colloidal assemblies. *Angew. Chem. Int. Ed.* **56**, 7817–7821 (2017).
25. A. Altemose, A. J. Harris, A. Sen, Autonomous formation and annealing of colloidal crystals induced by light-powered oscillations of active particles. *ChemSystemsChem* **2**, e1900021 (2020).
26. M. Ibele, T. E. Mallouk, A. Sen, Schooling behavior of light-powered autonomous micromotors in water. *Angew. Chem. Int. Ed.* **48**, 3308–3312 (2009).
27. Q. Wang, C. Zhou, L. Huang, W. Wang, "Ballistic" waves among chemically oscillating micromotors. *Chem. Commun.* **57**, 8492–8495 (2021).
28. A. Bricard, J.-B. Caussin, N. Desreumaux, O. Dauchot, D. Bartolo, Emergence of macroscopic directed motion in populations of motile colloids. *Nature* **503**, 95–98 (2013).
29. H. Wang, M. Pumera, Coordinated behaviors of artificial micro/nanomachines: From mutual interactions to interactions with the environment. *Chem. Soc. Rev.* **49**, 3211–3230 (2020).
30. F. Mou, J. Zhang, Z. Wu, S. Du, Z. Zhang, L. Xu, J. Guan, Phototactic flocking of photochemical micromotors. *iScience* **19**, 415–424 (2019).
31. C. Wu, J. Dai, X. Li, L. Gao, J. Wang, J. Liu, J. Zheng, X. Zhan, J. Chen, X. Cheng, M. Yang, J. Tang, Ion-exchange enabled synthetic swarm. *Nat. Nanotechnol.* **16**, 288–295 (2021).
32. X. Liang, F. Mou, Z. Huang, J. Zhang, M. You, L. Xu, M. Luo, J. Guan, Hierarchical microswarms with leader–follower-like structures: Electrohydrodynamic self-organization and multimode collective photoresponses. *Adv. Funct. Mater.* **30**, 1908602 (2020).
33. H. Xie, M. Sun, X. Fan, Z. Lin, W. Chen, L. Wang, L. Dong, Q. He, Reconfigurable magnetic microrobot swarm: Multimode transformation, locomotion, and manipulation. *Sci. Robot.* **4**, eaav8006 (2019).
34. J. Yu, B. Wang, X. Du, Q. Wang, L. Zhang, Ultra-extensible ribbon-like magnetic microswarm. *Nat. Commun.* **9**, 3260 (2018).
35. I. Farkas, D. Helbing, T. Vicsek, Mexican waves in an excitable medium. *Nature* **419**, 131–132 (2002).
36. K. Gentile, S. Maiti, A. Brink, B. Rallabandi, H. A. Stone, A. Sen, Silver-based self-powered pH-sensitive pump and sensor. *Langmuir* **36**, 7948–7955 (2020).
37. J.-Z. Guo, H. Cui, W. Zhou, W. Wang, Ag nanoparticle-catalyzed chemiluminescent reaction between luminol and hydrogen peroxide. *J. Photochem. Photobiol. A* **193**, 89–96 (2008).
38. C. Torres, E. Crastechini, F. Feitosa, C. Pucci, A. Borges, Influence of pH on the effectiveness of hydrogen peroxide whitening. *Oper. Dent.* **39**, E261–E268 (2014).
39. C. Zhou, H. P. Zhang, J. Tang, W. Wang, Photochemically powered AgCl Janus micromotors as a model system to understand ionic self-diffusiophoresis. *Langmuir* **34**, 3289–3295 (2018).
40. S. Ebbens, D. A. Gregory, G. Dunderdale, J. R. Howse, Y. Ibrahim, T. B. Liverpool, R. Golestanian, Electrokinetic effects in catalytic platinum-insulator Janus swimmers. *Europhys. Lett.* **106**, 58003 (2014).
41. A. Brown, W. Poon, Ionic effects in self-propelled Pt-coated Janus swimmers. *Soft Matter* **10**, 4016–4027 (2014).
42. A. T. Brown, W. C. K. Poon, C. Holm, J. de Graaf, Ionic screening and dissociation are crucial for understanding chemical self-propulsion in polar solvents. *Soft Matter* **13**, 1200–1222 (2017).
43. Y. Peng, P. Xu, S. Duan, J. Liu, J. L. Moran, W. Wang, Generic rules for distinguishing autophoretic colloidal motors. *Angew. Chem. Int. Ed.* **61**, e202116041 (2022).
44. J. L. Anderson, Colloid transport by interfacial forces. *Annu. Rev. Fluid Mech.* **21**, 61–99 (1989).
45. J. Katuri, W. E. Uspal, M. N. Popescu, S. Sánchez, Inferring non-equilibrium interactions from tracer response near confined active Janus particles. *Sci. Adv.* **7**, eabd0719 (2021).
46. M. Chen, Z. Lin, M. Xuan, X. Lin, M. Yang, L. Dai, Q. He, Programmable dynamic shapes with a swarm of light-powered colloidal motors. *Angew. Chem. Int. Ed.* **60**, 16674–16679 (2021).
47. J. L. Moran, J. D. Posner, Role of solution conductivity in reaction induced charge auto-electrophoresis. *Phys. Fluids* **26**, 042001 (2014).
48. J. M. Rogers, A. D. McCulloch, A collocation-Galerkin finite element model of cardiac action potential propagation. *IEEE Trans. Biomed. Eng.* **41**, 743–757 (1994).
49. S. Sinha, S. Sridhar, *Patterns in Excitable Media: Genesis, Dynamics, and Control* (CRC Press, 2014).
50. M. A. Sánchez-Farrán, A. Borhan, A. Sen, V. H. Crespi, Coupling between colloidal assemblies can drive a bistable-to-oscillatory transition. *ChemSystemsChem* **2**, e1900036 (2020).
51. S. Nakata, M. Nomura, H. Yamamoto, S. Izumi, N. J. Suematsu, Y. Ikura, T. Amemiya, Periodic oscillatory motion of a self-propelled motor driven by decomposition of H_2O_2 by catalase. *Angew. Chem. Int. Ed.* **129**, 879–882 (2017).

52. N. J. Suematsu, Y. Mori, T. Amemiya, S. Nakata, Oscillation of speed of a self-propelled Belousov–Zhabotinsky droplet. *J. Phys. Chem. Lett.* **7**, 3424–3428 (2016).
53. R. María-Hormigos, A. Escarpa, B. Goudeau, V. Ravaine, A. Perro, A. Kuhn, Oscillatory light-emitting biopolymer based Janus microswimmers. *Adv. Mater. Interfaces* **7**, 1902094 (2020).
54. A. Kaminaga, V. K. Vanag, I. R. Epstein, Wavelength halving in a transition between standing waves and traveling waves. *Phys. Rev. Lett.* **95**, 058302 (2005).
55. J. Yan, M. Han, J. Zhang, C. Xu, E. Luijten, S. Granick, Reconfiguring active particles by electrostatic imbalance. *Nat. Mater.* **15**, 1095–1099 (2016).
56. Z. T. Liu, Y. Shi, Y. Zhao, H. Chaté, X.-q. Shi, T. H. Zhang, Activity waves and freestanding vortices in populations of subcritical Quincke rollers. *Proc. Natl. Acad. Sci. U.S.A.* **118**, e2104724118 (2021).
57. X. Chen, C. Zhou, Y. Peng, Q. Wang, W. Wang, Temporal light modulation of photochemically active, oscillating micromotors: Dark pulses, mode switching, and controlled clustering. *ACS Appl. Mater. Interfaces* **12**, 11843–11851 (2020).
58. P. H. Jones, O. M. Maragò, G. Volpe, *Optical Tweezers: Principles and Applications* (Cambridge Univ. Press, 2015).
59. J. Friend, L. Y. Yeo, Microscale acoustofluidics: Microfluidics driven via acoustics and ultrasonics. *Rev. Mod. Phys.* **83**, 647–704 (2011).
60. N.-T. Nguyen, S. T. Wereley, S. A. M. Shaegh, *Fundamentals and Applications of Microfluidics* (Artech House, 2019).
61. R. Kubota, M. Makuta, R. Suzuki, M. Ichikawa, M. Tanaka, I. Hamachi, Force generation by a propagating wave of supramolecular nanofibers. *Nat. Commun.* **11**, 3541 (2020).
62. K. Sano, X. Wang, Z. Sun, S. Aya, F. Araoka, Y. Ebina, T. Sasaki, Y. Ishida, T. Aida, Propagating wave in a fluid by coherent motion of 2D colloids. *Nat. Commun.* **12**, 6771 (2021).
63. C. Lozano, C. Bechinger, Diffusing wave paradox of phototactic particles in traveling light pulses. *Nat. Commun.* **10**, 2495 (2019).
64. L. M. Goldenberg, J. Wagner, J. Stumpe, B.-R. Paulke, E. Görnitz, Simple method for the preparation of colloidal particle monolayers at the water/alkane interface. *Langmuir* **18**, 5627–5629 (2002).
65. X.-h. Bai, W. Li, X.-s. Du, P. Zhang, Z.-d. Lin, Synthesis of spherical silver particles with micro/nanostructures at room temperature. *Compos. Commun.* **4**, 54–58 (2017).
66. S. Zhang, E. Y. Scott, J. Singh, Y. Chen, Y. Zhang, M. Elsayed, M. D. Chamberlain, N. Shakiba, K. Adams, S. Yu, C. M. Morshead, P. W. Zandstra, A. R. Wheeler, The optoelectronic microrobot: A versatile toolbox for micromanipulation. *Proc. Natl. Acad. Sci.* **116**, 14823–14828 (2019).
67. Z. Liang, D. Teal, D. Fan, Light programmable micro/nanomotors with optically tunable in-phase electric polarization. *Nat. Commun.* **10**, 5275 (2019).
68. S. Palagi, A. G. Mark, S. Y. Reigh, K. Melde, T. Qiu, H. Zeng, C. Parmeggiani, D. Martella, A. Sanchez-Castillo, N. Kapernaum, F. Giesselmann, D. S. Wiersma, E. Lauga, P. Fischer, Structured light enables biomimetic swimming and versatile locomotion of photoresponsive soft microrobots. *Nat. Mater.* **15**, 647–653 (2016).
69. J. Arlt, V. A. Martinez, A. Dawson, T. Pilizota, W. C. K. Poon, Painting with light-powered bacteria. *Nat. Commun.* **9**, 768 (2018).

Acknowledgments: We acknowledge helpful discussions with I. Aronson and D. Velegol from Penn State University, and M. Yang from the Institute of Physics, CAS. We also thank P. Xu for the help with particle tracking and J. Tang and B. Dong for the information on fluorescence dye. **Funding:** X.C., Y.P., C.Z., and W.W. are financially supported by the Science Technology and Innovation Program of Shenzhen (JCYJ20190806144807401, JCYJ20210324121408022, and RCYX20210609103122038) and the National Natural Science Foundation of China (11774075). Y.X. and H.P.Z. are supported by the National Natural Science Foundation of China (12074243 and 11774222). **Author contributions:** X.C., C.Z., and Y.P. performed the experiments. Y.X. performed the numerical simulations. K.L., Y.X., and H.P.Z. designed and installed the optical setup. X.C., Y.X., H.P.Z., and W.W. wrote the manuscript. H.P.Z. and W.W. designed and supervised the project. Conceptualization: X.C., Y.X., C.Z., H.P.Z., and W.W. Methodology: X.C., C.Z., Y.X., and K.L. Investigation: X.C., C.Z., Y.X., and Y.P. Visualization: X.C., Y.X., C.Z., and Y.P. Supervision: H.P.Z. and W.W. Writing: X.C., Y.X., H.P.Z., and W.W. Writing—review and editing: X.C., Y.X., H.P.Z., and W.W. **Competing interests:** The authors declare that they have no competing interests. **Data and materials availability:** All data needed to evaluate the conclusions in the paper are present in the paper and/or the Supplementary Materials.

Submitted 31 December 2021
Accepted 8 April 2022
Published 25 May 2022
10.1126/sciadv.abn9130

ScienceAdvances

Unraveling the physiochemical nature of colloidal motion waves among silver colloids

Xi ChenYankai XuChao ZhouKai LouYixin PengH. P. ZhangWei Wang

Sci. Adv., 8 (21), eabn9130. • DOI: 10.1126/sciadv.abn9130

Science Advances (ISSN) is published by the American Association for the Advancement of Science. 1200 New York Avenue NW, Washington, DC 20005. The title *Science Advances* is a registered trademark of AAAS.